HHS Public Access

Author manuscript

Retina. Author manuscript; available in PMC 2017 December 01.

Published in final edited form as:

Retina. 2016 December ; 36(Suppl 1): S127–S136. doi:10.1097/IAE.0000000000001325.

Hyperspectral Autofluorescence Imaging of Drusen and Retinal Pigment Epithelium in Donor Eyes with Age-Related Macular Degeneration

Yuehong Tong, PhD[1], **Tal Ben Ami, MD**[1], **Sungmin Hong, MSc**[2], **Rainer Heintzmann, PhD**[3,4], **Guido Gerig, PhD**[2], **Zsolt Ablonczy, PhD**[5], **Christine A. Curcio, PhD**[6], **Thomas Ach, MD**[7] **[co-senior author]**, and **R. Theodore Smith, MD PhD**[1] **[co-senior author]**

[1]Department of Ophthalmology, New York University School of Medicine, New York, New York

[2]Department of Computer Science and Engineering, New York University Tandon School of Engineering, Brooklyn, New York

[3]Leibniz Institute of Photonic Technology, Jena, Germany

[4]Institute of Physical Chemistry and Abbe Center of Photonics, Friedrich Schiller University of Jena, Jena, Germany

[5]Department of Ophthalmology, Medical University of South Carolina, Charleston, South Carolina

[6]Department of Ophthalmology, University of Alabama School of Medicine, Birmingham, Alabama

[7]Department of Ophthalmology, University Hospital of Würzburg, Würzburg, Germany

Abstract

Purpose—To elucidate the molecular pathogenesis of age-related macular degeneration (AMD) and interpretation of fundus autofluorescence (AF) imaging, we identified spectral AF characteristics of drusen and retinal pigment epithelium (RPE) in donor eyes with AMD.

Methods—Macular RPE/Bruch's membrane (BrM) flat mounts were prepared from 5 donor eyes with AMD. In 12 locations (1–3/eye), hyperspectral AF images in 10-nm-wavelength steps were acquired at 2 excitation wavelengths (λ_{ex} 436 nm, 480 nm). A non-negative tensor factorization algorithm was used to recover 5 abundant emission spectra and their corresponding spatial localizations.

Results—At λ_{ex} 436 nm, we consistently localized a novel spectrum (SDr) with a peak emission near 510 nm in drusen and sub-RPE deposits. Abundant emission spectra seen previously (S0 in BrM and S1, S2, and S3 in RPE lipofuscin/melanolipofuscin (L/ML), respectively), also appeared in AMD eyes, with the same shapes and peak wavelengths as in normal tissue. L/ML spectra

Correspondence/reprint requests: R. Theodore Smith, MD, PhD. Department of Ophthalmology, New York University School of Medicine, 462 First Avenue – NBV 5N18, New York, NY 10016, USA; roland.smith@nyumc.org.

The paper was presented at the International Retinal Imaging (IRIS IV) Symposium at the Ronald Reagan UCLA Medical Center, March 19, 2016.

The other authors have no proprietary interests to disclose.

localizations in AMD eyes varied widely in their overlap with drusen, ranging from none to complete.

Conclusions—An emission spectrum peaking at ~510 nm (λ_{ex} 436 nm) appears to be sensitive and specific for drusen and sub-RPE deposits. One or more abundant spectra from RPE organelles exhibit characteristic relationships with drusen.

Keywords

age-related macular degeneration; autofluorescence; Bruch's membrane; drusen; fluorophores; hyperspectral imaging; lipofuscin; non-negative tensor factorization; retinal pigment epithelium; subretinal pigment epithelium deposits

Introduction

Age-related macular degeneration (AMD) is the leading cause of vision loss in the industrialized world.[1]_ENREF_1 Drusen are hallmark early signs of AMD.[2] They are extracellular deposits between the basal lamina of the retinal pigment epithelium (RPE) and the inner collagenous layer of Bruch's membrane (BrM). Drusen are categorized into soft and hard based on their clinical appearance, with soft drusen specific for the macula and for AMD.[3] Over the long term (5–20 years), even hard drusen can progress to soft drusen and clinical AMD.[4, 5] To date, the only treatment for early AMD with drusen is antioxidant supplementation for just a subset of these patients.[6–8]

Our understanding of drusen biogenesis and therapeutically significant pathways affected by AMD would be accelerated by a comprehensive profile of drusen composition.[9] Drusen, as revealed by *ex vivo* histochemistry, mass spectrometry, and X-ray microanalysis, have strong components of lipids, including esterified and unesterified cholesterol and phosphatidylcholine, calcium phosphate in the form of hydroxyapatite, and scores of proteins, including apolipoproteins E, B, and J, vitronectin, tissue inhibitor of metalloproteinase-3 (TIMP-3), and many proteins in the complement pathway (e.g., complement factor H and C9).[10–16] Some components are reflected in genetic associations, especially complement (innate immunity) and TIMP-3 (regulation of extracellular matrix).[17] The potential impact of new methods for identifying druse molecular components *in vivo* cannot be overestimated.

Abnormal fundus autofluorescence (AF) is another important clinical biomarker for understanding retinal degenerations, including AMD, and the source fluorophores, primarily in RPE, have been intensely investigated.[2, 18–20] The autofluorescent intracellular organelles containing these sources, lipofuscin (L), have further been implicated beyond biomarker status as an *agent* of AMD and Stargardt disease, and yet strong clinical evidence refutes this hypothesis.[18, 21, 22]_ENREF_19_ENREF_16 Clearly, the chemical composition of L is important to understanding human retinal disease.

However, the knowledge gap about major RPE fluorophores in the human *macula* remains enormous, largely because commonly used analytic methods are not capable of spatial localization.[19, 20] Thus, when the precise localization of imaging mass spectrometry (IMS)

revealed that the major L fluorophore, A2E,[20] is abundant in the *periphery* in humans,[23] corroborating earlier chromatographic evidence,[24] the source(s) of the strong macular AF signal became uncertain. It is worth also noting in this context the seminal findings of Marmorstein et al.,[25] who recorded the total spectral AF of RPE, BrM, drusen, and sub-RPE deposits in accurate histologic cross-section and found significant differences between normal and AMD donors. However, no attempt was made to discover individual tissue sources in these sections, and no subsequent experiments using isolated human lipofuscin AF have provided macular localizations.[26]

To begin to address this huge gap in our understanding, we have proposed hyperspectral imaging analysis as a tool to identify individual AF *spectra* of component fluorophores within the total tissue AF emission, en route to discovering the fluorophores themselves. Originally employed in satellite imagery for water resource control,[27, 28] hyperspectral imaging is now widely applied in food quality and safety control,[29, 30] forensic medicine,[31–33] and biomedicine.[34, 35] By providing spatially resolved spectral imaging, hyperspectral imaging has great potential for image-guided surgeries[36, 37] and disease detection_ENREF_34[38–40] and monitoring.[41, 42] Hyperspectral imaging may be employed in either the commonly used reflectance mode or the state-of-the-art AF mode. In reflectance mode, we have used it to study macular pigment[43] and retinal oximetry.[44] In AF mode, we have used it to recover the AF spectra of RPE and BrM in normal donor eyes.[45, 46] It is thus potentially one of the most precise methods to analyze retinal disease involving RPE.[47]

Hyperspectral imaging devices record at each pixel *total* AF, a mixture of spectra dependent on the sources present, as a function of wavelength (λ). The entire imaging dataset is thus a 3-dimensional hyperspectral data cube, or “hypercube,” of emission data with 1 spectral dimension (λ) and 2 spatial dimensions (x,y from the tissue). The spatial dimension images are stacked by emission wavelength to form the hypercube (Fig 1). The hypercube can be explored with advanced, unsupervised mathematical tools to identify dominant spectral signatures. The process of resolving these spectra and finding their spatial distributions is called “hyperspectral image unmixing.” We developed a software package based on non-negative tensor factorization (NTF) to unmix hyperspectral images into the major components in the targeted sample. NTF is a multiple excitation dataset formulation of the more familiar non-negative matrix factorization (NMF).[48]

In this study, we applied our algorithm to hyperspectral AF images of AMD donor tissue to retrieve the spectra of drusen. We found a novel spectrum that was both sensitive and specific for drusen and sub-RPE deposits. Previously, Marmorstein et al. demonstrated a total spectral emission of drusen in normal and AMD eyes without identifying drusen-specific individual components.[25] Herein we demonstrate, by hyperspectral unmixing, the first AF spectrum that localizes to drusen and sub-RPE deposits *only* (specific) and is also detected *throughout* these structures (sensitive). RPE spectra previously identified by our group in normal tissues were also identified in these AMD tissues, overlapping somewhat with drusen. Spectral information from drusen and RPE can provide novel insights into the biogenesis of drusen, which in turn can motivate new diagnostic imaging devices and facilitate *in vivo* molecular discovery in AMD.

Methods

Samples

RPE/BrM flat mounts were prepared from 5 AMD donor tissues, as described.[49] Tissues were from 2 female and 3 male donors (age range 81–90 years). AMD stage was defined at the time of accession using stereo color photographs and the criteria of the Alabama Age-Related Maculopathy Grading System (≥1 druse larger than 125 μm in diameter or an area of pigment change 500 μm in diameter) and confirmed by expert evaluation of the entire flat-mounted macula.[50, 51]_ENREF_45 Some tissues were also examined using *ex vivo* spectral-domain optical coherence tomography (acquired with the Spectralis OCT, Heidelberg Engineering, Heidelberg, Germany) to confirm the presence of drusen and abnormal hypo/hyperAF. Of the 5 donors, one had early AMD, one had GA, and 3 had exudative AMD. Twelve tissue locations with drusen (1 to 3 per eye) were selected.

Image Acquisition

Hyperspectral AF emission images were acquired from each tissue from 420 to 720 nm (spectral channel width: 10 nm) with a hyperspectral camera (Nuance FX, Caliper LifeSciences, Waltham, MA, USA) attached to a wide-field epi-fluorescence microscope (Axio Imager A2, Carl Zeiss, Jena, Germany) with 2 band-pass filter cubes for AF excitation (excitation/emission = 436/460 nm and excitation/emission = 480/510 nm; Chroma Technology Corp., Bellows Falls, VT, USA), an external mercury arc light source (X-Cite 120Q, Lumen Dynamics Group, Inc., Mississauga, Ontario, Canada), and a 40X oil objective (numerical aperture = 1.4). One hypercube was acquired at each of 2 excitation wavelengths (λ_{ex} 436 nm and λ_{ex} 480 nm).

Image Registration

All hypercubes were inspected for precise registration of the 2-dimensional spatial slices. In some instances, there was a small linear drift within a hypercube and/or a single linear shift between the hypercubes associated with the 2 excitation wavelengths. These shifts were presumably due to displacements in microscope optics during image acquisition. Subtle non-linear “barrel”-type distortions were also observed between slices at different emission wavelengths, presumably due to chromatic aberrations. These shifts were corrected with rigid body and nonlinear registration algorithms, respectively.[52, 53]

Image Analysis

Hyperspectral AF images were analyzed with our published NTF algorithm.[45] In brief, NTF is an unsupervised machine-learning technique. NTF for each tissue was initialized with 4 Gaussian-shaped spectra from RPE and one from BrM for each excitation hypercube to search for 5 abundant spectra from each hypercube. Hypercubes at each excitation were solved *simultaneously* to recover the 5 spectra and component localizations in each tissue. Spectra were recovered in 5 pairs at λ_{ex} 436 nm and λ_{ex} 480 nm, 1 pair for each abundant source. Tissue localizations from a given source were thus identical. Localizations were displayed as abundance images in false colors. Because the 3 fundamental novel RPE spectra previously identified in normal tissues[45, 46] were also identified in AMD tissues, we

retained the nomenclature and visualization formats from these prior reports, for ease of comparison: S1, green; S2, blue; S3, red; and S0 = BrM, gray. The new spectrum of drusen, SDr, was assigned the color azure.

Tissue Localizations

Images of human ***RPE/BrM tissues*** in flat mounts and in fundus view represent projection images of multiple biologically and compositionally distinct layers. At any x,y location, we visualize a sum of all layers present in the z-axis, which are RPE, basal laminar deposit (if present), basal linear deposit/drusen (if present), BrM, and choriocapillary endothelium. Herein, basal laminar deposit (BLamD) and basal linear deposit (BLinD) are collectively called sub-RPE deposits, as definitive separation requires transmission electron microscopy or high-resolution light microscopy.[54] We use the word “co-localize” to indicate signals that derive from the same x,y,z point within a specific layer compartment (i.e., 2 signals within a druse). We use the word “overlay” or “overlap” to indicate signals that occupy the same x,y points but different z points due to different layer compartments (i.e., L granules overlying a druse). Further, 3 RPE organelle populations are significant for AF imaging: L, melanolipofuscin (ML), and melanosomes (M). In particular, combined L and ML populations appear to account for the different emission spectra at excitation wavelengths used in this study.

Results

Twelve locations with drusen from 5 AMD donors were imaged using wide-field epi-fluorescence microscopy. A total of 25 drusen were analyzed: 12 small (≤63 μm diameter), 8 intermediate (64–124 μm), and 5 large (≥125 μm). Typical composite (RGB) AF images are shown in Fig 2C, D, annotated for tissue components and compared to corresponding bright-field images of melanin distribution (Fig 2A, B). Figs 3A and 3B illustrate spectra recovered from tissues shown in Fig 2A, C and 2C, D, respectively. Recovered spectra are in pairs representing 1 fluorophore family excited at both λ_{ex} 436 nm and λ_{ex} 480 nm. Figs 4A and 4B show the recovered abundances from these same tissues, 1 for each pair of spectra. Each abundance image indicates the spatial origin (localization) of the corresponding AF spectrum in histologic detail.

The Specific AF Spectrum of Drusen and Sub-RPE Deposits

The emission spectra (SDr) of drusen and sub-RPE deposits from 2 donor tissues are the azure curves in Figs 3A and 3B (spectral output panels). Note that the corresponding azure abundance images (Figs 4A and 4B) show localization of these signals strictly to the drusen and sub-RPE deposits, with no localization to RPE or BrM. Thus the SDr signal is specific to drusen and sub-RPE deposits. The observed spectral peak of SDr at λ_{ex} 436 nm was 510 nm in 10/12 tissues (Fig 3B), with the other 2 peaks at 500 nm (Fig 3A) and 490 nm (not shown). There were also consistently weaker emissions from drusen excited at λ_{ex} 480 nm (Figs 3A and 3B), with most peaks appearing at 520 nm. A few appeared at 540 nm, and 1 appeared at 530 nm. These were similarly shaped signatures that appeared to be 100% specific for drusen and sub-RPE deposits in all 12 tissues. In addition, in many tissues SDr was weakly and irregularly present in areas of intact RPE, which we interpreted to signify

deposits under the RPE in these locations. Because all drusen and sub-RPE deposits exhibited the same SDr signal, i.e., it did not vary from tissue to tissue or with drusen size, SDr was also completely sensitive for these lesions (Figs 4A and 4B).

AF Spectra of the RPE in AMD Tissues with Drusen

We previously identified, in normal tissues, 3 spectra attributable to RPE L/ML as S1, S2, and S3.[45] In 9/12 AMD tissues with drusen in this study, S1 at λ_{ex} 436 nm peaked similarly and strongly at 530±10 nm (Figs 3A and 3B, solid green curves). The second abundant constituent of normal RPE, S2, was also represented in AMD tissues, peaking at 570 nm with either excitation, a slightly shorter wavelength than in normal tissues (575 nm). The third abundant spectral constituent of normal RPE, S3, was also present in AMD tissues. Like S3 in normal eyes, S3 in AMD eyes had a broad tri-modal spectrum either with a central flat peak around 620 nm and secondary shoulders at 575 and 650 nm (Figs 3A and 3B, red curves in spectral outputs at either excitation) or, as is more common for S3 in normal tissues excited at λ_{ex} 436 nm, with the actual peak around 650 nm and secondary shoulders at 575 and 620 nm[45]; these cases were fairly evenly divided. At λ_{ex} 480 nm, the peak was near 620 nm in 9/12 cases. This spectrum appeared to localize to melanin within RPE (Figs 4A and 4B, red images). However, at λ_{ex} 436 nm, S3 in RPE of normal eyes was non-zero across the visible spectrum, whereas in AMD eyes it was non-zero only in longer wavelengths and declined to zero between 550 and 600 nm (Figs 3A and 3B). Another finding in RPE from normal eyes was the frequent splitting of S1 into 2 spectra, S1A and S1B. This was not observed in these AMD eyes, because our algorithm was designed to recover only 5 spectra total, which were S0, S1, S2, S3, and SDr in each case.

Co-localization of RPE Fluorophores with Drusen and Sub-RPE Deposits

The relationship of RPE signal sources to drusen was complex. Although drusen and sub-RPE deposits had 1 unique spectral signature, the drusen, but *not* the sub-RPE deposits, also exhibited additional AF that was resolved as combinations of RPE spectra S1–S3. The proportion of the fluorophore families S1–S3 within drusen was essentially *constant* within a given tissue and seemed to favor the spectra most abundant in the RPE itself. For example, in Fig 4A, S2 (blue) is moderately abundant in the druse, whereas S1 and S3 (green and red) are much less so, in proportion to the total spectral strengths in the NMF output (Fig 3A). In contrast, in Fig 4B, S1 (green) is abundant in the druse, but S2 and S3 are nearly absent, likewise in rough proportion to the total tissue spectral strengths (Fig 3B). This pattern was seen in 10/12 tissue samples. With regard to sub-RPE deposits, however, RPE spectra were minimally present. In Fig 4B, no RPE fluorophore is detected in the sub-RPE deposits (lower right).

Fluorophores of the RPE Adjacent to or Overlying Drusen

It is also possible that localization of an RPE fluorophore to drusen represents overlap. Thus, in Fig 4B, what appears to be localization of S2 and S3 to drusen is in fact attributable to L granules *overlying* the drusen, perhaps in effaced RPE, as noted in Fig 2B. Further, S2 and S3 are intense within haloes immediately surrounding, but not coinciding with, the drusen, perhaps attributable to RPE cells draped over druse margins. Returning to Fig 4A, we see that S3, barely present in the druse itself, is strong within RPE immediately surrounding the

druse. In this case, rather than a uniform halo, S3 is present more in the L/ML compartment of individual cells.

The AF Spectrum of BrM in AMD Tissues with Drusen

In normal tissues, BrM spectral abundances localized to areas of bare BrM and shone through RPE nuclei.[46] The spectrum peaked at 490 nm at λ_{ex} 436 nm, being non-zero throughout the full 420–720 nm range. In AMD tissues, BrM spectral abundances still localized correctly at a markedly lower intensity relative to normal than the RPE signals S1–S3 in the same tissues. Further, the BrM spectrum was usually flat and confined to the 420–500 nm range, without a well-defined peak.

Discussion

The appearance of macular soft drusen is a hallmark of AMD. Treatment with antioxidants can slow progression to advanced AMD and is the only known safe therapy.[55] However, despite recognition of many druse components,[10–13, 56] pathways of drusen biogenesis are incompletely known. The lipid accumulation on BrM that begins with BLinD and proceeds to drusen is best understood,[57] and the role and origin of the other components are less clear. Which components are of systemic vs. RPE origin is uncertain, because the RPE expresses genes for many druse components.[58]

This study represents a step toward identifying the AF components of drusen and sub-RPE deposits. For all stages of AMD and drusen sizes examined, a novel AF emission spectrum SDr, which appears to be highly specific and sensitive for drusen and sub-RPE deposits, consistently appeared at an emission maximum near 510 nm at λ_{ex} 436 nm. Furthermore, the 3 major L/ML fluorophore families S1–S3, previously identified in normal tissue,[46] can be identified in drusen in AMD tissues. Therefore, the AF spectra of drusen appear to be a mixture of the drusen-specific spectrum SDr and normal L/ML spectra. The fact that SDr occupies a range shared by the RPE and BrM spectra suggests that the source drusen fluorophore(s) may be of BrM or RPE origin. Remarkably, however, we also have demonstrated that SDr localizes *only* to drusen and sub-RPE deposits and is *not* shared by BrM or RPE. Thus, if the drusen fluorophore originates from BrM or RPE, it has undergone chemical and spectral change. The fact that drusen and sub-RPE deposits share some, but not all, components[59] also has a spectral interpretation in these results. The spectral signature SDr, which is sensitive and specific for both these structures, must arise from components that are shared between them. However, the L signatures that appear in drusen but not in sub-RPE deposits must arise from components of drusen not shared by sub-RPE deposits, such as the extracellular matrix proteins in BLamD. In other words, our data suggest that the components of drusen not shared by sub-RPE deposits are at least in part of RPE L origin.

Of note, we could not determine, without confocal microscopy and precise z-axis control, which of the sub-RPE deposits, BLamD (thickened basal lamina) or BLinD (also called diffuse drusen),[60] was responsible for the spectrum SDr that was shared with drusen. Because BLinD is soft druse material in a thin (<3 μm) and diffusely distributed form, a reasonable hypothesis is that the signal source was BLinD. In general, in order to understand

the fluorophores in any one compartment, it is necessary to understand what is in all the compartments, because the fluorophore signals are combined in the projection image.

The distribution of the 3 major L/ML fluorophore families in the drusen in a given tissue generally seemed to be dominated by the one with the strongest RPE signal overall, which varied between tissues. Clearly, the molecular mechanism by which RPE fluorophores incorporate in drusen is a significant open question. Finally, the relationship of RPE L/ML to the edges of drusen is complex, with L/ML granules overlying the drusen and/or high concentrations of fluorophores surrounding the drusen to form haloes in some cases. All of these points indicate an intimate relationship of the RPE and its fluorophores to the biogenesis of drusen that merits further research. These points are also relevant to the imaging interpretation of clinical AF images, in particular, the origin of hyperAF in and around drusen.

The RPE spectra were remarkably similar to those previously catalogued in normal tissue, although some variability in emission peaks and shapes may have been caused by sample preparation[61] or biologically significant differences in spectra between AMD and normal eyes. We identified the BrM spectrum in AMD tissues by its accurate co-localization to BrM, but it was markedly weaker than in normal tissues, perhaps due to blocking of the BrM signal by sub-RPE deposits or reduction of RPE-derived secretions as cellular health declines.

It is worth comparing our results with the seminal findings of Marmorstein et al.,[25] who recorded the spectral AF of RPE, BrM, drusen, and sub-RPE deposits, in normal and AMD donor tissue cross-sections, with 4 confocal laser excitation wavelengths (λ_{ex} 364, 488, 568, and 633 nm). No attempt was made to recover individual components in these tissue spectra. At λ_{ex} 488 nm, the wavelength for which we have comparison data, BrM emission in AMD was somewhat greater, and sub-RPE emission was somewhat less, than RPE L (Marmorstein et al., Fig 3B). Thus BrM AF intensity measured in AMD eyes was much higher relative to RPE L than our measured intensities. The most likely reason for this disparity is that the BrM emissions in our flat mounts were blocked by sub-RPE deposits and RPE. Examination of tissues like ours in cross-section should help resolve this question. For drusen and sub-RPE deposits in areas of our tissues devoid of RPE, signal intensities were comparable to the RPE L emissions (Fig 4B, SDr panel), in agreement with Marmorstein et al. However, for clarity it must be emphasized that the total emission spectra recorded by Marmorstein et al. is *not* the same as the *specific* signal SDr recovered herein by hyperspectral unmixing. As noted, NMF hyperspectral unmixing demonstrated that the total emission spectrum of drusen seen as a projection image is in fact a combination of SDr and various RPE fluorophores, as depicted in the abundance images (Fig 4B). The same caveats apply to other published data on the spectra of the RPE, whether in mice with pathology[62] or in humans with AMD.[26] However persuasive, these other unmixed data still all represent *total* emissions awaiting decomposition into contributions from individual fluorophores.

This study has several limitations. We do not have correlative cross-sectional histology or en face imaging linked to z-axis position to resolve questions about tissue sources in 3-dimensional space. Another limitation is that only 5 donor eyes were imaged and analyzed,

and imaging locations were not chosen by a systematic sampling scheme to reduce selection bias. We also analyzed drusen in samples from the near periphery, which may not represent macular drusen, although we found a consistent SDr signal across the regions examined.

A major strength of this technique is that the signals are extracted in an unbiased manner by a published automatic algorithm applied uniformly to each RPE/BrM tissue hyperspectral AF dataset. Thus, the excellent quality of the RPE/BrM flat mounts analyzed and the consistency of the drusen/sub-RPE deposit spectra allowed consistent hyperspectral recovery across 12 imaging locations and 25 distinct drusen deposits. Further, the shape of L/ML spectra in these AMD tissues was found essentially unchanged compared to RPE from normal donors characterized previously.[45, 46]

Conclusions

Our initial effort to decompose total AF emission tissue spectra of RPE, drusen, and sub-RPE deposits is a step towards molecular identification of these fluorophores *in vivo*. Such data may aid the understanding of AMD biogenesis. A clinical hyperspectral AF camera that could detect the earliest formation of drusen and sub-RPE deposits *in vivo* could provide an early warning for individuals at risk for AMD, as well as facilitate the development and monitoring of new therapies based on specific molecular defects. These advances would extend profound health and social benefits to our aging population.

Acknowledgments

The study was performed at New York University School of Medicine, New York, New York.

Supported by the National Institutes of Health/National Eye Institute (Bethesda, MD) grants R01 EY019065 (ZA), EY06109 (CAC), EY015520 (RTS), and EY021470 (RTS); a Foundation Fighting Blindness (Columbia, MD) Individual Investigator Research Award (RTS); unrestricted funds from Research to Prevent Blindness (New York, NY) (ZA, CAC, RTS); International Society for Eye Research (San Francisco, CA) 2014 von Sallmann Prize (CAC); EyeSight Foundation of Alabama (Birmingham, AL) (CAC); and German Research Foundation (Bonn, Germany) grants DFG Ac265/1-1 and DFG Ac265/2-1 (TA).

Christine A. Curcio is a consultant to Genentech (South San Francisco, CA, USA), Novartis (Basel, Switzerland), Merck (Kenilworth, NJ, USA), and Janssen Cell Therapy (Spring House, PA, USA). R. Theodore Smith is a consultant to Ocata Therapeutics (Marlborough, MA, USA).

References

1. Wong WL, Su X, Li X, et al. Global prevalence of age-related macular degeneration and disease burden projection for 2020 and 2040: a systematic review and meta-analysis. Lancet Glob Health. 2014; 2:e106–116. [PubMed: 25104651]
2. Smith RT, Chan JK, Busuoic M, et al. Autofluorescence characteristics of early, atrophic, and high-risk fellow eyes in age-related macular degeneration. Invest Ophthalmol Vis Sci. 2006; 47:5495–5504. [PubMed: 17122141]
3. Rudolf M, Clark ME, Chimento MF, et al. Prevalence and morphology of druse types in the macula and periphery of eyes with age-related maculopathy. Invest Ophthalmol Vis Sci. 2008; 49:1200–1209. [PubMed: 18326750]
4. Klein R, Klein BE, Knudtson MD, et al. Fifteen-year cumulative incidence of age-related macular degeneration: the Beaver Dam Eye Study. Ophthalmology. 2007; 114:253–262. [PubMed: 17270675]

5. Joachim N, Mitchell P, Burlutsky G, et al. The incidence and progression of age-related macular degeneration over 15 years: The Blue Mountains Eye Study. Ophthalmology. 2015; 122:2482–2489. [PubMed: 26383995]
6. Age-Related Eye Disease Study Research Group. A randomized, placebo-controlled, clinical trial of high-dose supplementation with vitamins C and E and beta carotene for age-related cataract and vision loss: AREDS report no. 9. Arch Ophthalmol. 2001; 119:1439–1452. [PubMed: 11594943]
7. Chew EY, Clemons TE, Agron E, et al. Long-term effects of vitamins C and E, beta-carotene, and zinc on age-related macular degeneration: AREDS report no. 35. Ophthalmology. 2013; 120:1604–1611.e1604. [PubMed: 23582353]
8. Age-Related Eye Disease Study 2 Research Group. Lutein + zeaxanthin and omega-3 fatty acids for age-related macular degeneration: the Age-Related Eye Disease Study 2 (AREDS2) randomized clinical trial. JAMA. 2013; 309:2005–2015. [PubMed: 23644932]
9. Hageman GS, Luthert PJ, Chong NH, et al. An integrated hypothesis that considers drusen as biomarkers of immune-mediated processes at the RPE-Bruch's membrane interface in aging and age-related macular degeneration. Prog Retin Eye Res. 2001; 20:705–732. [PubMed: 11587915]
10. Hageman GS, Mullins RF, Russell SR, et al. Vitronectin is a constituent of ocular drusen and the vitronectin gene is expressed in human retinal pigmented epithelial cells. FASEB J. 1999; 13:477–484. [PubMed: 10064614]
11. Curcio CA, Presley JB, Malek G, et al. Esterified and unesterified cholesterol in drusen and basal deposits of eyes with age-related maculopathy. Exp Eye Res. 2005; 81:731–741. [PubMed: 16005869]
12. Mullins RF, Russell SR, Anderson DH, Hageman GS. Drusen associated with aging and age-related macular degeneration contain proteins common to extracellular deposits associated with atherosclerosis, elastosis, amyloidosis, and dense deposit disease. FASEB J. 2000; 14:835–846. [PubMed: 10783137]
13. Crabb JW, Miyagi M, Gu X, et al. Drusen proteome analysis: an approach to the etiology of age-related macular degeneration. Proc Natl Acad Sci U S A. 2002; 99:14682–14687. [PubMed: 12391305]
14. Wang L, Clark ME, Crossman DK, et al. Abundant lipid and protein components of drusen. PLoS One. 2010; 5:e10329. [PubMed: 20428236]
15. Malek G, Li CM, Guidry C, et al. Apolipoprotein B in cholesterol-containing drusen and basal deposits of human eyes with age-related maculopathy. Am J Pathol. 2003; 162:413–425. [PubMed: 12547700]
16. Anderson DH, Ozaki S, Nealon M, et al. Local cellular sources of apolipoprotein E in the human retina and retinal pigmented epithelium: implications for the process of drusen formation. Am J Ophthalmol. 2001; 131:767–781. [PubMed: 11384575]
17. Fritsche LG, Chen W, Schu M, et al. Seven new loci associated with age-related macular degeneration. Nat Genet. 2013; 45:433–439. [PubMed: 23455636]
18. Hwang JC, Chan JW, Chang S, Smith RT. Predictive value of fundus autofluorescence for development of geographic atrophy in age-related macular degeneration. Invest Ophthalmol Vis Sci. 2006; 47:2655–2661. [PubMed: 16723483]
19. Wu Y, Fishkin NE, Pande A, et al. Novel lipofuscin bisretinoids prominent in human retina and in a model of recessive Stargardt disease. J Biol Chem. 2009; 284:20155–20166. [PubMed: 19478335]
20. Sparrow JR, Fishkin N, Zhou J, et al. A2E, a byproduct of the visual cycle. Vis Res. 2003; 43:2983–2990. [PubMed: 14611934]
21. Smith RT, Gomes NL, Barile G, et al. Lipofuscin and autofluorescence metrics in progressive STGD. Invest Ophthalmol Vis Sci. 2009; 50:3907–3914. [PubMed: 19387078]
22. Biarnes M, Arias L, Alonso J, et al. Increased fundus autofluorescence and progression of geographic atrophy secondary to age-related macular degeneration: The GAIN Study. Am J Ophthalmol. 2015; 160:345–353.e345. [PubMed: 25982972]
23. Ablonczy Z, Higbee D, Anderson DM, et al. Lack of correlation between the spatial distribution of A2E and lipofuscin fluorescence in the human retinal pigment epithelium. Invest Ophthalmol Vis Sci. 2013; 54:5535–5542. [PubMed: 23847313]

24. Bhosale P, Serban B, Bernstein PS. Retinal carotenoids can attenuate formation of A2E in the retinal pigment epithelium. Arch Biochem Biophys. 2009; 483:175–181. [PubMed: 18926795]
25. Marmorstein AD, Marmorstein LY, Sakaguchi H, Hollyfield JG. Spectral profiling of autofluorescence associated with lipofuscin, Bruch's membrane, and sub-RPE deposits in normal and AMD Eyes. Invest Ophthalmol Vis Sci. 2002; 43:2435–2441. [PubMed: 12091448]
26. Feldman TB, Yakovleva MA, Arbukhanova PM, et al. Changes in spectral properties and composition of lipofuscin fluorophores from human-retinal-pigment epithelium with age and pathology. Anal Bioanal Chem. 2015; 407:1075–1088. [PubMed: 25471291]
27. Govender M, Chetty K, Bulcock H. A review of hyperspectral remote sensing and its application in vegetation and water resource studies. Water SA. 2007; 33:145–151.
28. Adam E, Mutanga O, Rugege D. Multispectral and hyperspectral remote sensing for identification and mapping of wetland vegetation: a review. Wetlands Ecol Manage. 2010; 18:281–296.
29. Gowen AA, O'Donnell CP, Cullen PJ, et al. Hyperspectral imaging - an emerging process analytical tool for food quality and safety control. Trends Food Sci Tech. 2007; 18:590–598.
30. Feng YZ, Sun DW. Application of hyperspectral imaging in food safety inspection and control: a review. Crit Rev Food Sci Nutr. 2012; 52:1039–1058. [PubMed: 22823350]
31. Edelman GJ, Gaston E, van Leeuwen TG, et al. Hyperspectral imaging for non-contact analysis of forensic traces. Forensic Sci Int. 2012; 223:28–39. [PubMed: 23088824]
32. Edelman G, van Leeuwen TG, Aalders MC. Hyperspectral imaging for the age estimation of blood stains at the crime scene. Forensic Sci Int. 2012; 223:72–77. [PubMed: 22938693]
33. Malkoff DB, Oliver WR. Hyperspectral imaging applied to forensic medicine. Proc SPIE. 2000; 3920:108–116.
34. Carrasco O, Gomez R, Chainani A, Roper WE. Hyperspectral imaging applied to medical diagnoses and food safety. Proc SPIE. 2003; 5097:215–221.
35. Afromowitz MA, Callis JB, Heimbach DM, et al. Multispectral imaging of burn wounds: a new clinical instrument for evaluating burn depth. IEEE Trans Biomed Eng. 1988; 35:842–850. [PubMed: 3056848]
36. Wehner E, Thapa A, Livingston E, Zuzak K. NIR DLP hyperspectral imaging system for medical applications. Proc SPIE. 2011; 7932:793204.
37. Akbari H, Kosugi Y, Kojima K, Tanaka N. Blood vessel detection and artery-vein differentiation using hyperspectral imaging. Conf Proc IEEE Eng Med Biol Soc. 2009; 2009:1461–1464. [PubMed: 19963752]
38. Panasyuk SV, Yang S, Faller DV, et al. Medical hyperspectral imaging to facilitate residual tumor identification during surgery. Cancer Biol Ther. 2007; 6:439–446. [PubMed: 17374984]
39. Boucheron LE, Bi Z, Harvey NR, et al. Utility of multispectral imaging for nuclear classification of routine clinical histopathology imagery. BMC Cell Biol. 2007; 8(Suppl 1):S8. [PubMed: 17634098]
40. Sokolov K, Follen M, Richards-Kortum R. Optical spectroscopy for detection of neoplasia. Curr Opin Chem Biol. 2002; 6:651–658. [PubMed: 12413550]
41. Roblyer D, Richards-Kortum R, Sokolov K, et al. Multispectral optical imaging device for *in vivo* detection of oral neoplasia. J Biomed Opt. 2008; 13:024019. [PubMed: 18465982]
42. Roblyer D, Kurachi C, Gillenwater AM, Richards-Kortum R. *In vivo* fluorescence hyperspectral imaging of oral neoplasia. Proc SPIE. 2009; 7169:71690J.
43. Fawzi AA, Lee N, Acton JH, et al. Recovery of macular pigment spectrum *in vivo* using hyperspectral image analysis. J Biomed Opt. 2011; 16:106008. [PubMed: 22029355]
44. Gao L, Smith RT, Tkaczyk TS. Snapshot hyperspectral retinal camera with the image mapping spectrometer (IMS). Biomed Opt Express. 2012; 3:48–54. [PubMed: 22254167]
45. Smith RT, Post R, Johri A, et al. Simultaneous decomposition of multiple hyperspectral datasets: signal recovery of unknown fluorophores in the retinal pigment epithelium. Biomed Opt Express. 2014; 5:4171–4185. [PubMed: 25574430]
46. Ben Ami T, Tong Y, Bhuiyan A, et al. Spatial and spectral characterization of human retinal pigment epithelium fluorophore families by *ex vivo* hyperspectral autofluorescence imaging. Transl Vis Sci Technol Forthcoming.

47. Mordant DJ, Al-Abboud I, Muyo G, et al. Spectral imaging of the retina. Eye (Lond). 2011; 25:309–320. [PubMed: 21390065]
48. Lee DD, Seung HS. Learning the parts of objects by non-negative matrix factorization. Nature. 1999; 401:788–791. [PubMed: 10548103]
49. Ach T, Huisingh C, McGwin G Jr, et al. Quantitative autofluorescence and cell density maps of the human retinal pigment epithelium. Invest Ophthalmol Vis Sci. 2014; 55:4832–4841. [PubMed: 25034602]
50. Ach T, Tolstik E, Messinger JD, et al. Lipofuscin redistribution and loss accompanied by cytoskeletal stress in retinal pigment epithelium of eyes with age-related macular degeneration. Invest Ophthalmol Vis Sci. 2015; 56:3242–3252. [PubMed: 25758814]
51. Curcio CA, Medeiros NE, Millican CL. The Alabama Age-Related Macular Degeneration Grading System for donor eyes. Invest Ophthalmol Vis Sci. 1998; 39:1085–1096. [PubMed: 9620067]
52. Yoo TS, Ackerman MJ, Lorensen WE, et al. Engineering and algorithm design for an image processing Api: a technical report on ITK–the Insight Toolkit. Stud Health Technol Inform. 2002; 85:586–592. [PubMed: 15458157]
53. Rueckert D, Sonoda LI, Hayes C, et al. Nonrigid registration using free-form deformations: application to breast MR images. IEEE Trans Med Imaging. 1999; 18:712–721. [PubMed: 10534053]
54. Curcio CA, Millican CL. Basal linear deposit and large drusen are specific for early age-related maculopathy. Arch Ophthalmol. 1999; 117:329–339. [PubMed: 10088810]
55. Age-Related Eye Disease Study (AREDS) Research Group. A randomized, placebo-controlled, clinical trial of high-dose supplementation with vitamins C and E, beta carotene, and zinc for age-related macular degeneration and vision loss: AREDS Report No. 8. Arch Ophthalmol. 2001; 119:1417–1436. [PubMed: 11594942]
56. Sohn EH, Wang K, Thompson S, et al. Comparison of drusen and modifying genes in autosomal dominant radial drusen and age-related macular degeneration. Retina. 2015; 35:48–57. [PubMed: 25077532]
57. Curcio CA, Johnson M, Rudolf M, Huang JD. The oil spill in ageing Bruch membrane. Br J Ophthalmol. 2011; 95:1638–1645. [PubMed: 21890786]
58. Booij JC, Baas DC, Beisekeeva J, et al. The dynamic nature of Bruch's membrane. Prog Retin Eye Res. 2010; 29:1–18. [PubMed: 19747980]
59. Spaide RF, Curcio CA. Drusen characterization with multimodal imaging. Retina. 2010; 30:1441–1454. [PubMed: 20924263]
60. Green WR, Enger C. Age-related macular degeneration histopathologic studies. The 1992 Lorenz E. Zimmerman Lecture. Ophthalmology. 1993; 100:1519–1535. [PubMed: 7692366]
61. Yin D. Biochemical basis of lipofuscin, ceroid, and age pigment-like fluorophores. Free Radic Biol Med. 1996; 21:871–888. [PubMed: 8902532]
62. Palczewska G, Dong Z, Golczak M, et al. Noninvasive two-photon microscopy imaging of mouse retina and retinal pigment epithelium through the pupil of the eye. Nat Med. 2014; 20:785–789. [PubMed: 24952647]

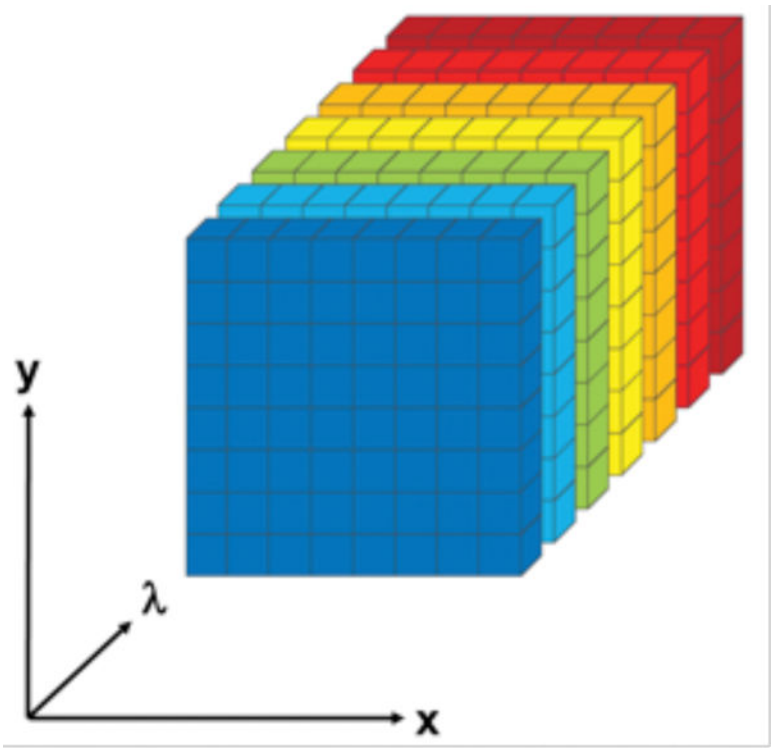

Fig 1. The hyperspectral autofluorescence emission data cube, or "hypercube"

The hypercube is acquired from a retinal pigment epithelium/Bruch's membrane tissue oriented in the x,y plane. For each emission wavelength λ, a 2-dimensional image of the tissue, or slice, is acquired, capturing all emissions of the tissue at that wavelength. The 2-dimensional slices (colored by emission wavelength for illustration) are stacked by λ to form the hypercube.

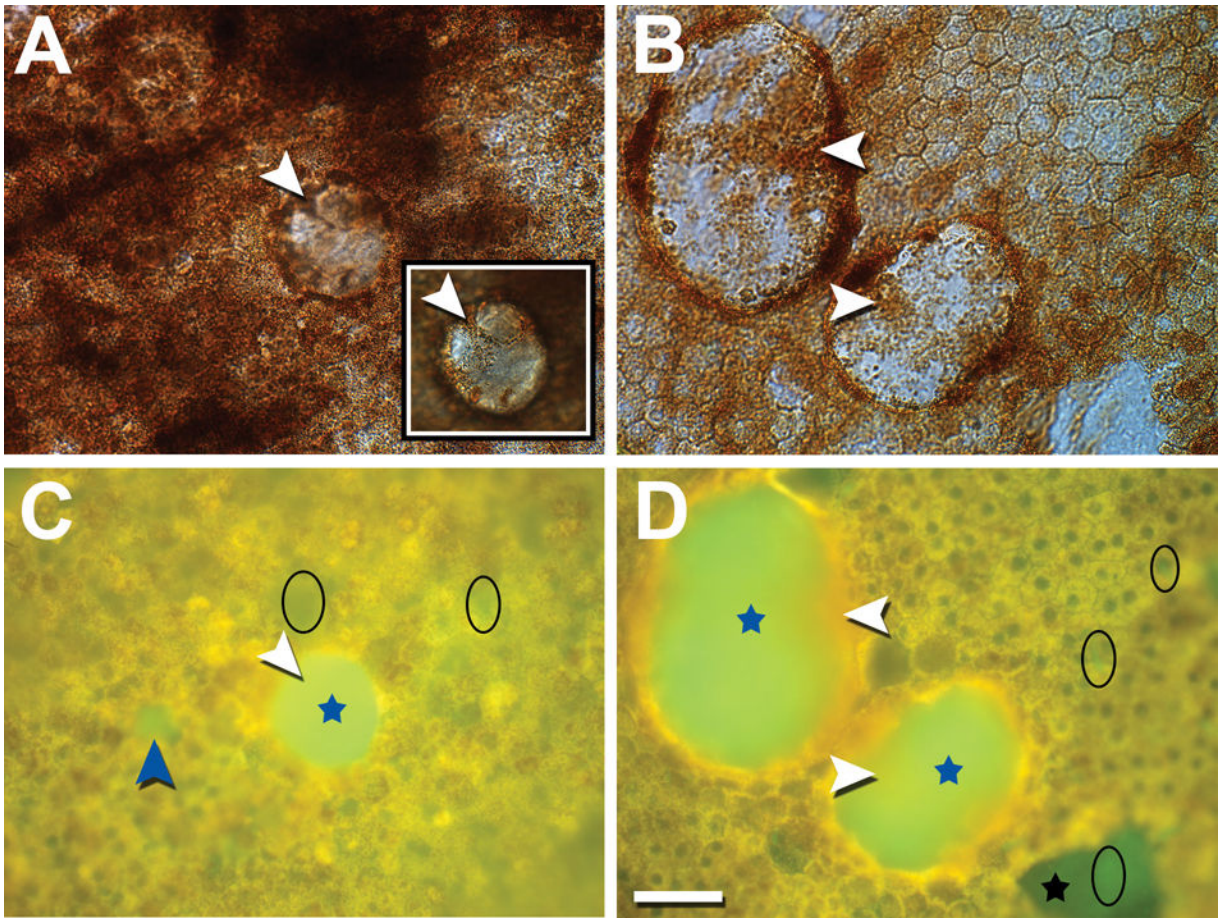

Fig 2. Bright field (A, B) and corresponding composite (RGB) hyperspectral autofluorescence (C, D) images of drusen (blue stars); retinal pigment epithelium (RPE)/Bruch's membrane (BrM) flat mounts from donors with age-related macular degeneration (AMD), viewed at λ_{ex} 436 nm

Lipofuscin, melanolipofuscin, and melanosomes are densely packed around drusen, while some of the granules (white arrowheads, **A, B**) are also visible on top of the drusen (inset in **A**, top of dome-shaped druse in focus). Granules overlying drusen show autofluorescence (AF) signal (white arrowheads, **C, D**). A small druse is visible in **C** (blue arrowhead). BrM without RPE cells (due to tissue processing) is visible in **D** (black star). The appearance is inhomogeneous, with some brighter green (black ellipse) within the dark green patch, consistent with sub-RPE deposits having a less intense AF signal than drusen. Similar areas (brighter than BrM, dimmer than drusen) can be found across the imaged locations (black ellipses). Donors: 84-year-old male, late exudative AMD (**A, C**); 81-year-old male, late non-exudative AMD (**B, D**). Scale bar: 50 μm.

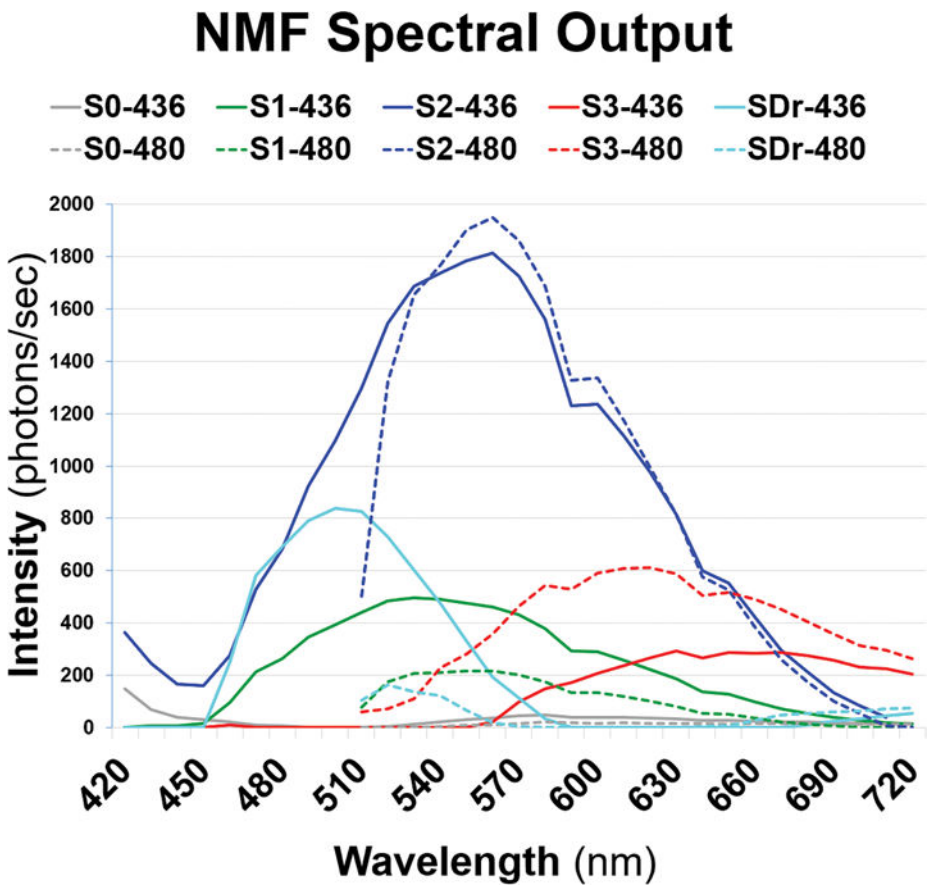

Fig 3A. Spectra recovered from tissue with small and intermediate drusen in Fig 2A, C

Emission spectra from λ_{ex} 436 nm (solid lines) and λ_{ex} 480 nm (dashed lines) reveal normal pairs of retinal pigment epithelium spectra S1, S2, and S3 (green, blue, and red) recovered from lipofuscin/melanolipofuscin. The drusen spectra (SDr) are in azure, peaking at 500 nm at λ_{ex} 436 nm. S0 (gray) is a Bruch's membrane spectrum, weak and truncated compared to normal tissue. (NMF = non-negative matrix factorization.)

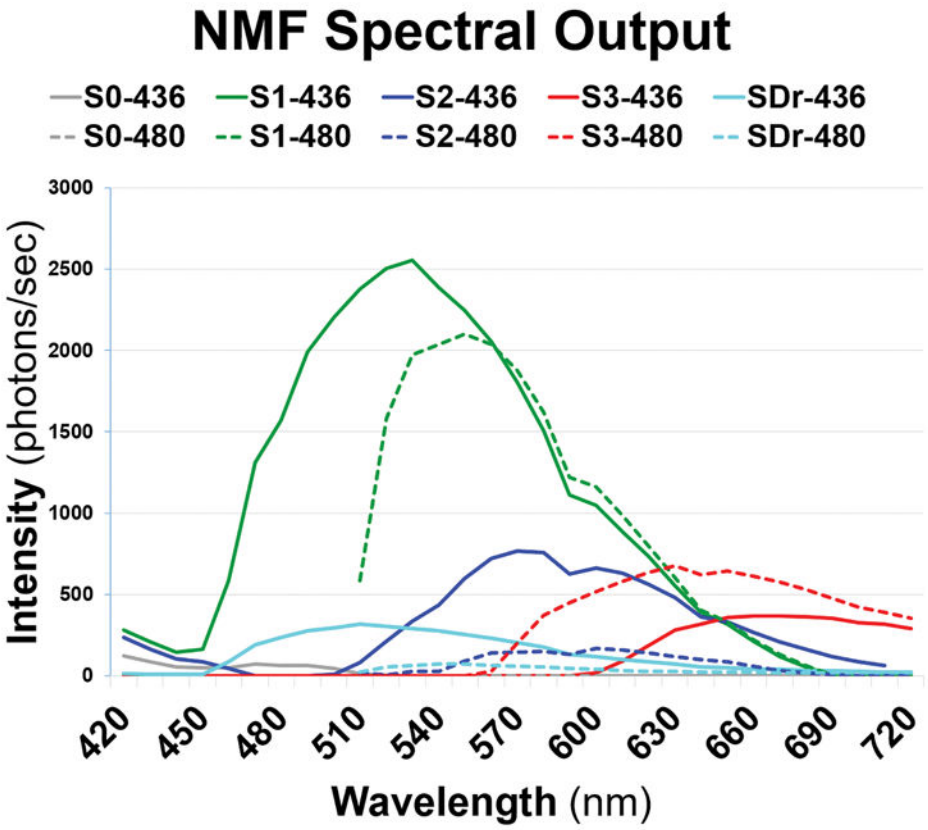

Fig 3B. Spectra recovered from tissue with large drusen in Fig 2B, D

Normal paired retinal pigment epithelium spectra S1, S2, and S3 (green, blue, and red) were recovered from lipofuscin/melanolipofuscin. The drusen spectra (SDr) are in azure, peaking at 510 nm at λ_{ex} 436 nm. A weak Bruch's membrane spectrum (S0, gray) was also found. (NMF = non-negative matrix factorization.)

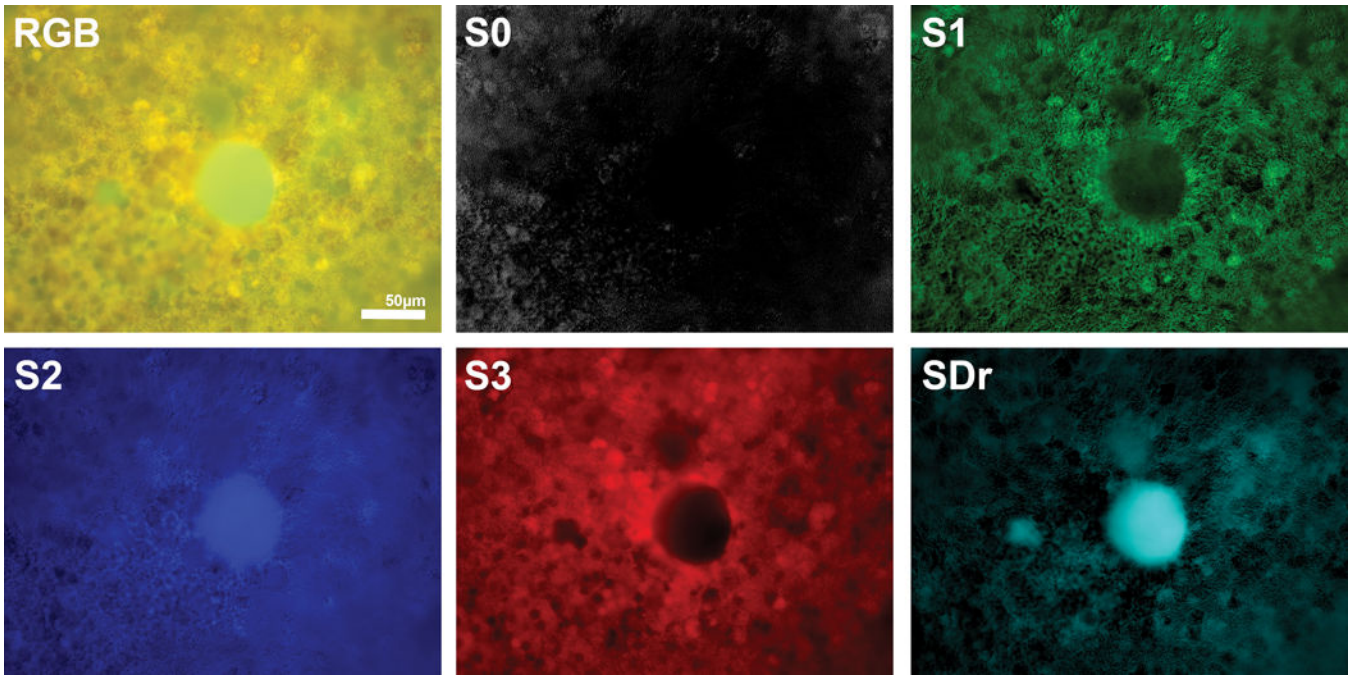

Fig 4A. Spectral localizations to small drusen and surrounding retinal pigment epithelium (RPE)

The upper left image is the composite RGB autofluorescence image in Fig 2C. S2 is abundant in the central druse but is not detectable in the tiny druse (blue arrowhead, Fig 2C). S1 and S3, however, are nearly absent from both, and their spectral strengths in the tissue overall (Fig 3A) are likewise much less than that of S2. S1 and S3, however, form strong haloes in the RPE around the larger druse and are also present in granules overlying it (annotated in Fig 2A, C). SDr strongly localizes to drusen. Irregular patches of additional SDr may correspond to sub-RPE deposits partly screened by the RPE itself. S0 (Bruch's membrane) shines through some RPE nuclei, as previously described, but does not localize to the drusen.

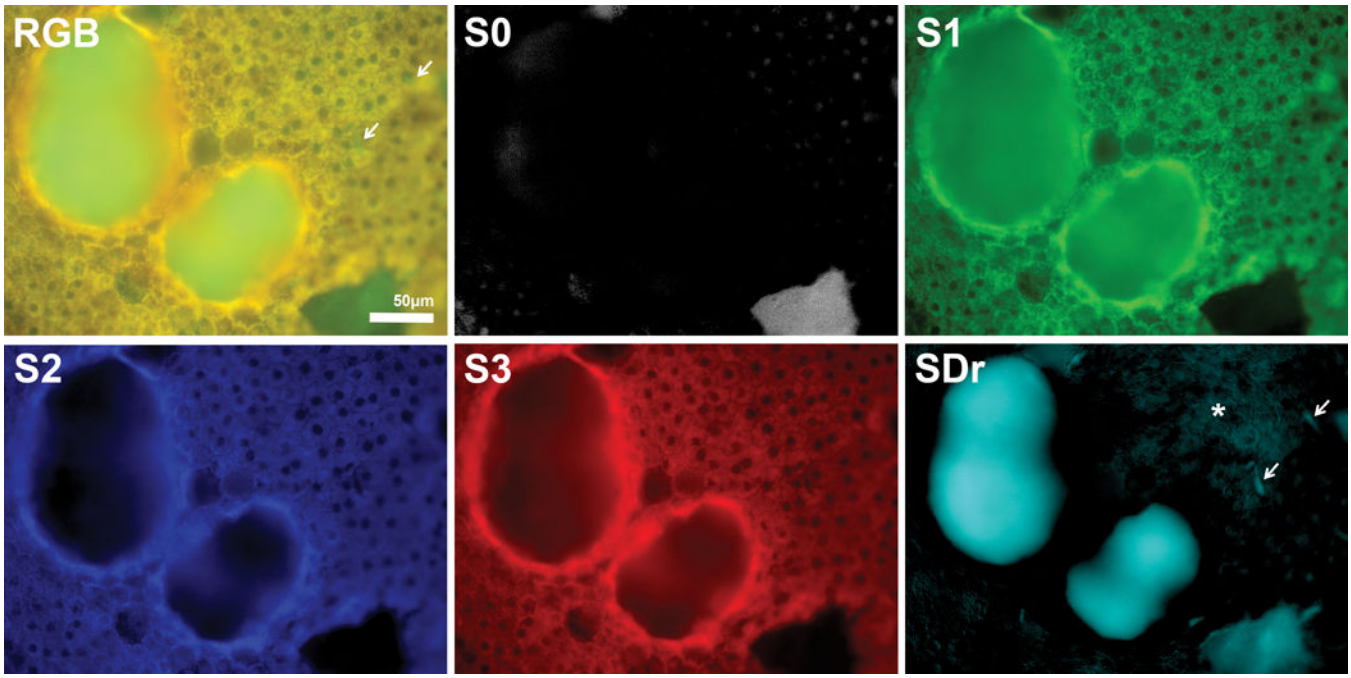

Fig 4B. Spectral localizations to large drusen and surrounding retinal pigment epithelium (RPE)

The upper left image is the composite RGB autofluorescence image in Fig 2D. S1 is moderately abundant in the drusen, whereas S2 and S3 are nearly absent. Their total spectral strengths in the tissue (Fig 3B) are likewise much less than that of S1. S2 and S3, however, form strong haloes in the RPE around the drusen, perhaps in RPE cells draped over the drusen margins. S2 and S3 are also present in granules overlying the drusen (annotated in Fig 2B, D). With regard to sub-RPE deposits and Bruch's membrane (BrM), which are both present in the patch in the lower right of the micrographs, S0 (BrM) and SDr (drusen and sub-RPE deposits) are both present. S0 localizes homogeneously exactly to the area of the patch, while SDr is inhomogeneous, appearing brighter in the areas of brighter green on the RGB image (Fig 2D), consistent with sub-RPE deposits. S0 also shines through several nuclei (upper right corner of S0 panel) but does not localize to the drusen. SDr strongly localizes to the drusen and to other flecks of sub-RPE deposit (white arrows) that are identified on the composite RGB image. Irregular patches of additional SDr (white asterisk) may correspond to sub-RPE deposits partly screened by the RPE itself. However, the abundances of RPE spectra S1, S2, and S3 are completely dark (spectra not present) in the area of BrM and sub-RPE deposit (lower right of the micrographs).